Darcian Natural Convection in Inclined Square Cavity Partially Filled Between the Central Square Hole Filled with a Fluid and Inside a Square Porous Cavity Filled with Nanofluid

A. I. Alsabery[1], H. Saleh[1†], I. Hashim[1,2] and S. H. Hussain[3]

[1] *School of Mathematical Sciences, Universiti Kebangsaan Malaysia, 43600 UKM Bangi, Selangor, Malaysia*
[2] *Research Institute Center for Modeling, Computer Simulation (RI/CM & CS), King Fahd University of Petroleum, Minerals Dhahran-31261, Saudi Arabia*
[3] *Head of Automobile Engineering Department, Al-Musayab College for Engineering and Technology, Babylon University, Babylon Province, Iraq*

Corresponding Author Email: *Dr.habibissaleh@gmail.com*

ABSTRACT

The problem of darcian natural convection in inclined square cavity partially filled between the central square hole filled with fluid and inside a square porous cavity filled with nanofluid is numerically studied using the finite element method. The left vertical wall is maintained at a constant hot temperature T_h and the right vertical wall is maintained at a constant cold temperature T_c, while the horizontal walls are adiabatic. The governing equations are obtained by applying the Darcy model and Boussinesq approximation. COMSOL's finite element method is used to solve the non-dimensional governing equations together with the specified boundary conditions. The governing parameters of this study are the Rayleigh number ($10^3 \leq Ra \leq 10^7$), the Darcy number ($10^{-5} \leq Da \leq 10^{-3}$), the fluid layer thickness ($0.4 \leq S \leq 0.8$) and the inclination angle of the cavity ($0° \leq \omega \leq 6\,0°$). The results for the values of the governing parameters in terms of the streamlines, isotherms and average Nusselt number will be presented. The convection is shown to be inhibited by the presence of the hole insert. The thermal property of the insert and the size have opposite influence on the convection. The results have possible applications in heat-removal and heat-storage fluid-saturated porous systems.

Keywords: Natural convection; Square cavity; Nanofluid; Interface; Darcy model.

NOMENCLATURE

|			
C_p	specific heat capacity	α	effective thermal diffusivity
Da	Darcy number	$\overline{\alpha}$	coefficient in Bevers
g	gravitational accleration		and Joseph's matching condition
k	thermal conductivity	β	thermal expansion coefficient
K	permeability of the porous medium	θ	dimensionless temperature
L	length of enclosure	μ	dynamic viscosity
$\overline{Nu}$	average Nusselt number	ν	kinematic viscosity
p	the pressure	ϕ	solid volume fraction
Pr	Prandtl number	ω	the inclination angle of the cavity
Ra	Rayleigh number	ρ	fluid density
S	dimensionless fluid layer thickness	*Subscript*	
T	temperature	c	cold
u, v	velocity components in the	bf	base fluid
	x- and y-directions	f	fluid
U, V	dimensionless velocity components	h	hot
	in the X-direction and Y-direction	nf	nanofluid
x, y & X, Y	space coordinates &	sp	solid nanoparticle
	dimensionless space coordinates		

1. INTRODUCTION

Natural convection fluid flow and heat transfer in porous media domains have received considerable attention over the past few years and importance is highlighted recently due to the wide range of environmental situations or industrial applications. These include geothermal systems, thermal insulation, filtration processes, ground water pollution, storage of nuclear waste, drying processes, solidification of castings, storage of liquefied gases, biofilm growth and fuel cells. problems of dealing with the fluid motions in the clear region and the porous medium have been extensively studied for many years. Beavers and Joseph (1967) presented a simple situation of the boundary conditions between a porous media and a homogeneous fluid. Poulikakos *et al.* (1986) considered high value of Rayleigh in natural convection in a fluid overlaying a porous bed using the Darcy model. Meanwhile, Beckermann *et al.* (1987) studied natural convection flow and heat transfer between a fluid layer and a porous layer inside a rectangular enclosure. Natural convection heat and mass transfer in solidification was studied by Beckermann *et al.* (1988). On the other hand, Chen and Chen (1989) investigated convective stability in a superposed fluid and porous layer when heated from below, while Le Breton *et al.* (1991) examined heat transfer and fluid flow through fibrous insulation. Singh and Thorpe (1995) presented a comparative study of different models on natural convection in a confined fluid and overlying porous layer. The problem of studying the solute exchange by convection within estuarine sediments was considered by Webster *et al.* (1996). Goyeau *et al.* (2003) discussed the problem of using one- or two domain formulations for conservation equations. Meanwhile, Gobin *et al.* (2005) studied a particular subclass of such problems where natural convection takes place in a confined enclosure partially filled with a porous medium. Nessrine *et al.* (2010) numerically analyzed the fluid flow and heat transfer in a pipe partially filled with porous media by using Brinkman-Forchheimer-Lapwood-extended Darcys model.

In addition to that, Vinogradov *et al.* (2011) applied the finite volume method to study the effect of the inclination angle on natural convection heat transfer in two-dimensional cavities filled with pure fluid. Bhattacharya and Das (2015) numerically considered the steady natural convective heat transfer in a square cavity by studying different values of Rayleigh and Nusselt numbers. Thermal fluids are very important for heat transfer in many industrial applications. The low thermal conductivity of conventional heat transfer fluids such as water and oils is the primary limitation in enhancing the performance and the compactness of many engineering electronic devices. Solid has a typically higher thermal conductivity than liquids. For example, copper (Cu) has a thermal conductivity of 700 time greater than that of water and 3000 greater than engine oil. An innovative and new technique to enhance heat transfer is by using solid particles in the base fluid (i.e. nanofluids) in the range of sizes 1050 nm (Chol 1995). Due to the small sizes and very large specific surface areas of the nanoparticles, nanofluids have superior properties like high thermal conductivity, minimal clogging in flow passages, longterm stability and homogeneity (Nasrin and Alim 2013). Thus, nanofluids have a wide range of potential applications such as in electronics, automotive, and nuclear applications where improved heat transfer or efficient heat dissipation is required. Ramiar *et al.* (2012) used the finite volume method to study the effects of axial conduction and variable properties on conjugate heat transfer in 2D microchannel filled with nanofluid. Arani *et al.* (2014) numerically investigated natural convection in a square cavity filled with nanofluids. Chamkha and Ismael (2014) conducted for the first time a numerical study to solve the problem of differentially heated and vertically partially layered porous cavity filled with nanofluids on natural convection by using the Darcy-Brinkman model. Zaraki *et al.* (2015) used finite-difference method to theoretically study the effects of size, shape, the type of nanoparticles, the type of base fluid, the working temperature of natural convection boundary layer heat and the mass transfer of nanofluids. Nevertheless, the study of natural convection fluid flow and heat transfer in a square cavity partially filled with nanofluid porous medium using the Darcy model has not been undertaken yet. The aim of this study is to investigate the darcian natural convection in inclined square cavity partially filled between the central square hole filled with a fluid and inside a square porous cavity filled with nanofluid.

2. MATHEMATICAL FORMULATION

Cosidering steady two-dimensional natural convection in a square cavity with length L, the cavity center inserted by square cavity filled with pure fluid with length W, while the remainder of the cavity $(L - W)$ is filled with nanofluid is illustrated in Fig. 1. The left vertical wall of the cavity is heated to constant temperature T_h
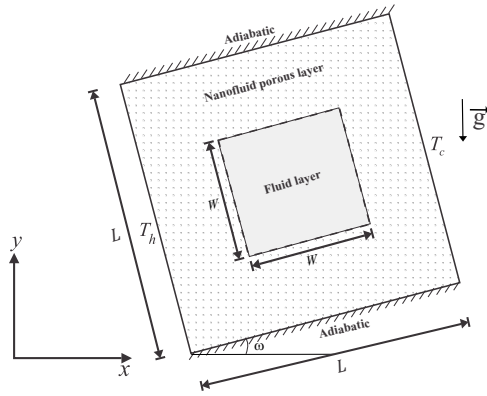
Fig. 1. Physical model of convection in a square porous cavity together with the coordinate system.

and the right vertical wall is maintained at constant cold temperature T_c, while the horizontal walls are adiabatic. The outer boundaries are assumed to be impermeable, while the fluid layer boundaries are assumed to be permeable. The pores filled with fluid composed from water–base nanofluids containing Ag, Cu or Al_2O_3 nanoparticles. According to the Boussinesq approximation, the fluid physical properties are constant except for the density. By considering these assumptions, the conservation equations for mass, Darcy and energy equations for steady natural convection for the fluid and the nanofluid layers will be considered separately. For the homogenous nanofluid (porous) layer, the continuity, momentum and energy equations can be written in dimensionless form as follows:

$$\frac{\partial U_{nf}}{\partial X} + \frac{\partial V_{nf}}{\partial Y} = 0, \tag{1}$$

$$U_{nf}\frac{\partial U_{nf}}{\partial X} + V_{nf}\frac{\partial U_{nf}}{\partial Y} = -(1-\phi)^{2.5}Ra_{bf}Da$$
$$\times \frac{(\rho\beta)_{nf}}{(\rho\beta)_{bf}} g\left(\theta_{nf} - \theta_c\right) \sin\omega, \tag{2}$$

$$U_{nf}\frac{\partial V_{nf}}{\partial X} + V_{nf}\frac{\partial V_{nf}}{\partial Y} = -(1-\phi)^{2.5}Ra_{bf}Da$$
$$\times \frac{(\rho\beta)_{nf}}{(\rho\beta)_{bf}} g\left(\theta_{nf} - \theta_c\right) \cos\omega, \tag{3}$$

$$U_{nf}\frac{\partial \theta_{nf}}{\partial X} + V_{nf}\frac{\partial \theta_{nf}}{\partial Y}$$
$$= \frac{\alpha_{nf}}{\alpha_{bf}}\left(\frac{\partial^2 \theta_{nf}}{\partial X^2} + \frac{\partial^2 \theta_{nf}}{\partial Y^2}\right). \tag{4}$$

The continuity, momentum and energy equations for the fluid layer are can be written in

dimensionless form as follows:

$$\frac{\partial U_f}{\partial X} + \frac{\partial V_f}{\partial Y} = 0, \tag{5}$$

$$U_f\frac{\partial U_f}{\partial X} + V_f\frac{\partial U_f}{\partial Y} = -\frac{\partial P_f}{\partial X}$$
$$+ \left(\frac{\partial^2 U_f}{\partial X^2} + \frac{\partial^2 U_f}{\partial Y^2}\right) + \frac{Ra}{Pr}\theta_f \sin\omega, \tag{6}$$

$$U_f\frac{\partial V_f}{\partial X} + V_f\frac{\partial V_f}{\partial Y} = -\frac{\partial P_f}{\partial Y}$$
$$+ \left(\frac{\partial^2 V_f}{\partial X^2} + \frac{\partial^2 V_f}{\partial Y^2}\right) + \frac{Ra}{Pr}\theta_f \cos\omega, \tag{7}$$

$$U_f\frac{\partial \theta_f}{\partial X} + V_f\frac{\partial \theta_f}{\partial Y} = \frac{1}{Pr}\left(\frac{\partial^2 \theta_f}{\partial X^2} + \frac{\partial^2 \theta_f}{\partial Y^2}\right) \tag{8}$$

where the following dimensionless variables have been used

$$X = \frac{x}{L},\ Y = \frac{y}{L},\ U = \frac{Lu}{\alpha},\ V = \frac{Lv}{\alpha},$$
$$\theta_{nf} = \frac{T_{nf} - T_c}{T_h - T_c},\ \theta_f = \frac{T_f - T_c}{T_h - T_c}. \tag{9}$$

Here U and V are the dimensionless velocity components along X-axes and Y-axes, $Ra_{bf} = gK\rho_{bf}\beta_{bf}(T_h - T_c)L/(\mu_{bf}\alpha_{bf})$ is the Rayleigh number for both the fluid and the porous layer, $Da = K/L^2$ is the Darcy number for both the fluid and the porous layer and $Pr = \nu_f/\alpha_f$ is the Prandtl number for both the fluid and the porous layer. The dimensionless boundary conditions of Eqs. (2)–(8) are:

$$\theta_{nf} = \theta_f\quad =\quad 1 \text{ at } X = 0 \tag{10}$$
$$\theta_{nf} = \theta_f\quad =\quad 0 \text{ at } X = 1 \tag{11}$$
$$\frac{\partial \theta_{nf}}{\partial Y} = \frac{\partial \theta_f}{\partial Y}\quad =\quad 0 \text{ at } Y = 0,\ Y = 1 \tag{12}$$

and at the interface by using the matching conditions proposed by Beavers and Joseph (1967)

$$\frac{\partial U}{\partial X} = \bar{\alpha}(U^+ - V^-)/\sqrt{Da},$$
$$\theta\mid_{X=s^+} = \theta\mid_{X=s^-},$$
$$k_{nf}\frac{\partial T}{\partial X}s^+ = k_f\frac{\partial T}{\partial X}s^-. \tag{13}$$

where in our study the value of $\bar{\alpha}$ fix at 1.

α_{nf} is the effective thermal diffusivity of the nanofluids, ρ_{nf} is the effective density of the nanofluids and μ_{nf} is the effective dynamic viscosity of the nanofluids and, which are defined as

$$\alpha_{nf} = \frac{k_{nf}}{(\rho Cp)_{nf}},\ \rho_{nf} = (1-\phi)\rho_{bf} + \phi\rho_{sp},$$
$$\mu_{nf} = \frac{\mu_{bf}}{(1-\phi)^{2.5}}, \tag{14}$$

Where, the heat capacitance of the nanofluids given is

$$(\rho Cp)_{nf} = (1-\phi)(\rho Cp)_{bf} + \phi(\rho Cp)_{sp} \qquad (15)$$

The thermal expansion coefficient of the nanofluids can be determined by

$$\beta_{nf} = (1-\phi)(\beta)_{bf} + \phi\beta_{sp}, \qquad (16)$$

$$(\rho\beta)_{nf} = (1-\phi)(\rho\beta)_{bf} + \phi(\rho\beta)_{sp}. \qquad (17)$$

The thermal conductivity based on Maxwell-Garnett's (MG) model is given below:

$$\frac{k_{nf}}{k_{bf}} = \frac{k_{sp} + 2k_{bf} - 2\phi(k_{bf} - k_{sp})}{k_{sp} + 2k_{bf} + \phi(k_{bf} - k_{sp})} \qquad (18)$$

The local average Nusselt number evaluated at the hot vertical wall of the nanofluid porous layer is:

$$\overline{Nu}_{nf} = \int_0^1 \left[-\left(\frac{k_{nf}}{k_{bf}}\right) \frac{\partial \theta_{nf}}{\partial X} \right] dY. \qquad (19)$$

3. NUMERICAL METHOD AND VALIDATION

Based on the Galerkin finite element method (GFEM), the governing equations subject to the boundary conditions are solved numerically using the CFD software package COMSOL multiphysics, a general-application solver and simulation of interconnected partial differential equation. This flexible platform contains the art numerical algorithms and visualization tools bundled together with an easy to use interface. The COMSOL's finite element method was applied to solve the two momentum equations in nanofluid layer Eqs. (2, 3), the heat transfer in nanofluid layer Eq. (4), the two momentum equations in fluid layer Eqs. (6, 7) and the heat transfer in fluid layer Eq. (8) subject to the boundary conditions Eqs. (10)–(13).

In this investigation, mesh generation on square cavity is made by using graph grid. By considering the accuracy, finer, extra fine and extremely fine mesh sizes were selected for all the computations done in this study. As a validation, we compared our figures with what were presented by Singh and Thorpe (1995) as shown in Fig. 2. Fig. 2. shows the comparison between present results and results present by Singh and Thorpe (1995) for $Ra = 10^5$, $Da = 10^{-5}$, $\phi = 0$ and $S = 0$. It is clear from this comparison that the present results are in excellent agreement with the corresponding results.

4. RESULTS AND DISCUSSION

In this section, we present numerical results for the streamlines of nanofluid/fluid-layer and isotherms of nanofluid/fluid-layer with various values of Rayleigh number ($10^3 \leq Ra \leq 10^7$), Darcy number ($10^{-5} \leq Da \leq 10^{-3}$), the fluid

(a)

(b)
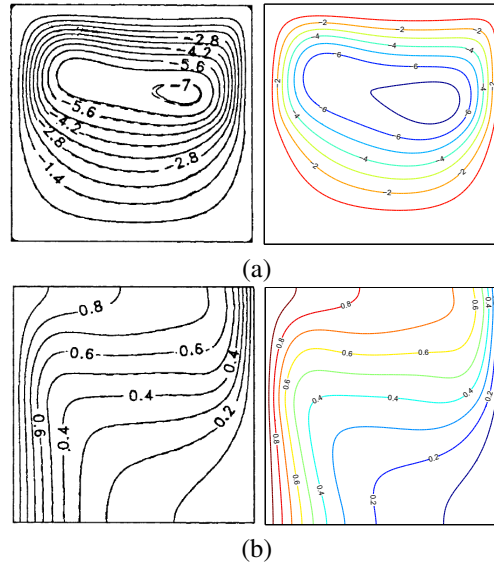
Fig 2. Streamlines (a), Singh and Thorpe (1995) (left), present study (right), isotherms (b), Singh and Thorpe (1995) (left), present study (right) for $Ra = 10^5$, $Da = 10^{-5}$, $\phi = 0$ and $S = 0.5$.

Table 1 Thermo-physical properties of water with Ag, Cu and Al$_2$O$_3$

Properties Physical	Water	Ag	Cu	Al$_2$O$_3$
Cp (J/kgK)	4179	235	383	765
ρ (kg/m^3)	997.1	10500	8954	3600
k (Wm^{-1}K^{-1})	0.6	429	400	46
$\beta \times 10^{-5}$ (1/K)	21	5.4	1.67	0.63

Table 2 Effective thermal conductivity values of nanofluids at $300°K$

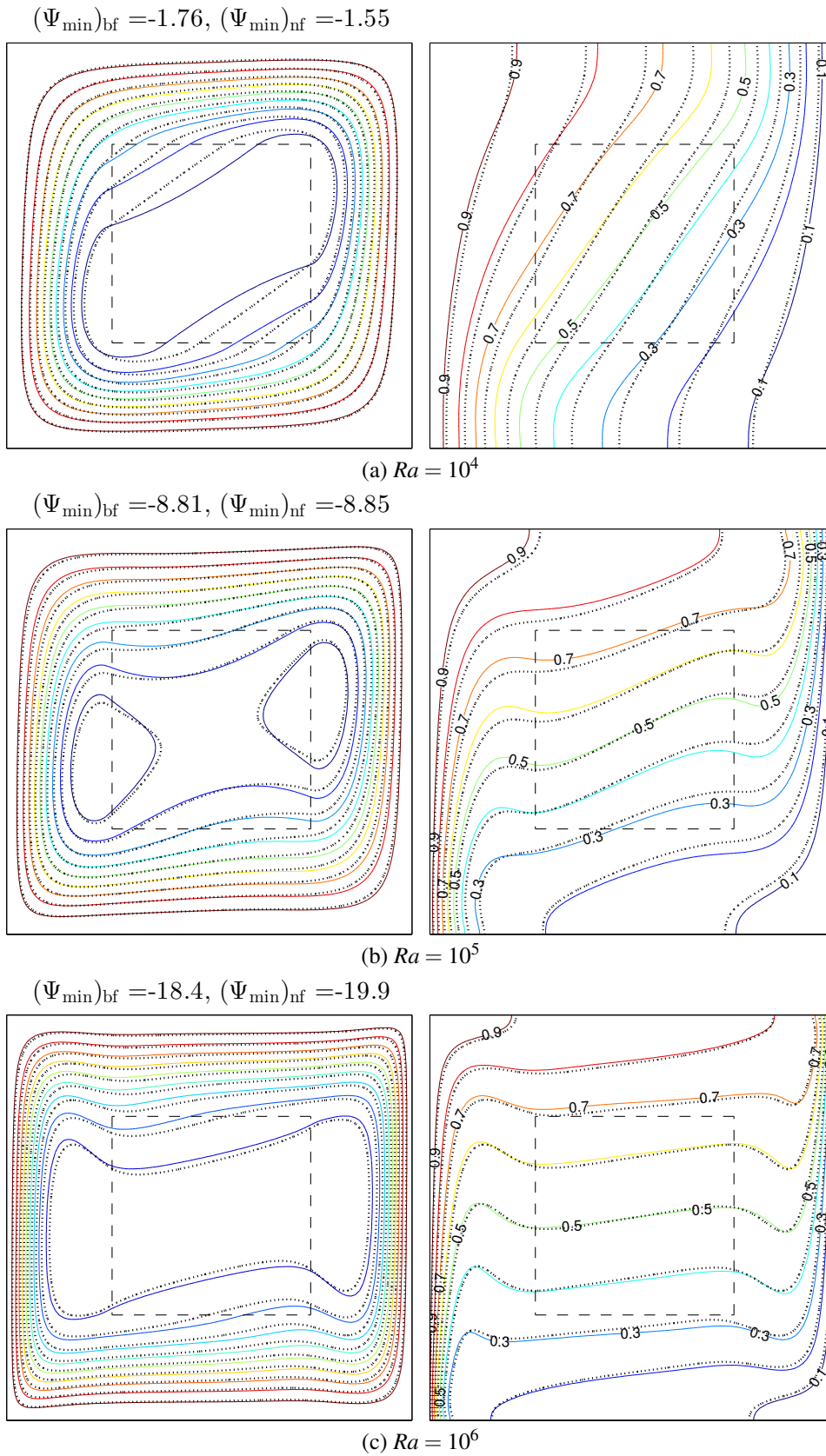| Nanofluid	ϕ	k_{nf}
Water-Ag	0.05	0.694
	0.10	0.799
	0.15	0.916
	0.20	1.048
Water-Cu	0.05	0.694
	0.10	0.799
	0.15	0.916
	0.20	1.047
Water-Al$_2$O$_3$	0.05	0.691
	0.10	0.791
	0.15	0.903
	0.20	1.029

layer thickness ($0.4 \leq S \leq 0.8$), the inclination angle of the cavity ($0° \leq \omega \leq 60°$) and Prandtl number $Pr = 6.2$. The values of the average Nusselt number were calculated for various values of Ra, ϕ and ω. Before we move on to the discussion of the results it is worthwhile knowing about values of quantities of base fluid, nanoparticles and effective thermal conductivity values concerning a nanofluid. These are presented in the Tables 1 and 2. From Table 2 it is apparent that the thermal conductivity, k_{nf}, increase with increase in ϕ but the rates at which they increase determines their role in either enhancing or diminishing heat transfer.

Figure 3 shows the effects of various Rayleigh numbers on the streamlines (left) and isotherms (right) for water–Cu nanoparticles with Darcy number ($Da = 10^{-3}$), fluid layer thickness ($S = 0.5$) and inclination angle of the cavity ($\omega = 0°$). Within the scope of the present study, Fig. 3(a) demonstrates the streamlines and isotherm patterns at a lower value Rayleigh number (10^4). The heated left wall of the cavity caused the flow inside the cavity to rise and the flow began to move from the left wall (hot) (nanofluid partition) to the right wall (cold) with infiltrates into the fluid layer, descending along the right wall, and then ascending again at the hot wall, creating a clockwise rotating cell inside the cavity (fluid partition). The flow circulation of the streamlines cells for nanofluid are bigger than that for pure fluid. When the streamlines circulated as vortices in the clockwise direction (negative signs of Ψ), the strength of the flow circulation was presented by Ψ_{min}. The conduction heat transfer forced the isotherms patterns within the nanofluid layer to take an almost diagonal shape while, the convection mode heat transfer affected the isotherms patterns within the fluid layer appeared as diagonal lines on the vertical walls. As the nanoparticle volume fraction is applied ($\phi = 0.05$), the circulation intensity decreases (see Ψ_{min} values) due to the lower value of the Rayleigh number (10^4). The intensity of the streamlines within the nanofluid layer increases as Ra increases, due to the permeability of the nanofluid layer. The increase in the strength of the flow circulation can be observed with the increase in the values of Ra (see Ψ_{min} values). As the nanoparticle volume fraction is applied ($\phi = 0.05$), the circulation intensity increases (see Ψ_{min} values) due to the increase in the thermal conductivity of nanofluid, as shown in Fig. 3(b). The streamlines circulation cell inside the cavity shrinks and becomes two oval cells on the interface walls. The distortion of the isotherms pattern is enhanced as the

Rayleigh number increases ($Ra = 10^5$), the vertical isotherms pattern in the nanofluid tended to become diagonal lines, while into the fluid layer the diagonal lines tend to turned to the horizontal shaped. A significant modification in the streamlines and isotherm patterns presented by Fig. 3(c), at higher Ra, the two circulation cells on the interface are disappeared, the streamlines intensity increases near to the vertical walls (lett and right). The flow circulation of the streamlines cells for nanofluid become smaller than that for pure fluid.

The effects of Darcy number on the streamlines (left) and isotherms (right) are illustrated in Fig. 4. for water–Cu nanoparticles, $Ra = 10^5$, $S = 0.5$ and $\omega = 0°$. Fig. 4(a) depicts the effect of changing the flow motion with the boundary conditions set at a lower Da value of ($Da = 10^{-5}$). As the nanoparticle volume fraction is applied ($\phi = 0.05$), the circulation intensity decreases (see Ψ_{min} values) due to the lower value of Darcy number (10^{-5}). Increasing Da to 10^{-4} leads to the increase in the intensity of streamlines and as a result, the strength of the flow circulation increases (see Ψ_{min} values). The flow circulation of the streamlines cells for nanofluid become closer to that of pure fluid. The diagonal isotherm patterns movement into the fluid layer is significantly effected by the convection and the isotherm patterns close to the interface tend to take a horizontal shape as Da increases, as presented in Fig. 4(b). Increasing Da to a higher value (10^{-3}) enhances the streamlines. As a result, the two streamlines circulation cells on the interface walls tend to increase and transform into a trapezoidal shape. The strength of the flow circulation increases by applying the nanoparticle volume fraction ($\phi = 0.05$), (see Ψ_{min} values) due to the increases in the thermal conductivity of the nanofluid with high Da. The distortion of the isotherms pattern is enhanced because the isotherms patterns within the fluid layer tend to take an almost horizontal shape while the isotherms patterns near the vertical walls (hot and cold wall) appear with vertical lines, as shown in Fig. 4(c).
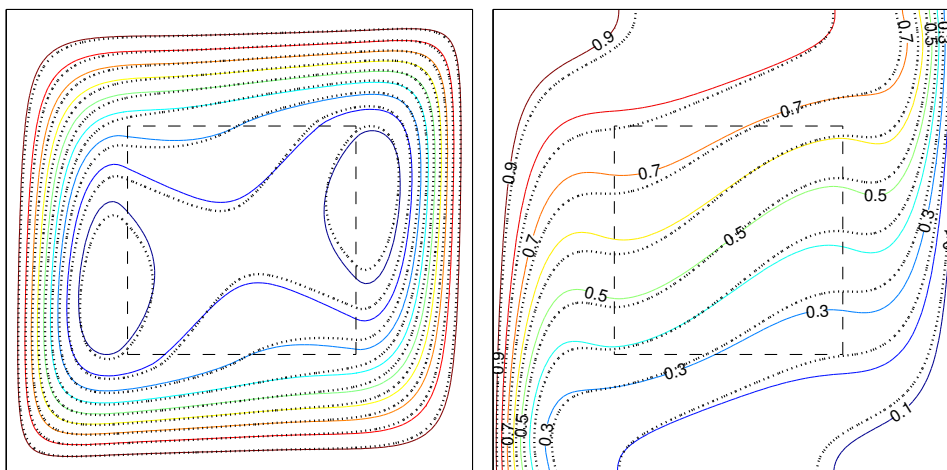
Figure 5 depicts the effect of fluid layer thickness on the streamlines (left) and isotherms (right) for water–Cu nanoparticles, $Ra = 10^5$, Darcy number ($Da = 10^{-3}$) and inclination angle of the cavity ($\omega = 0°$). The effect of lower S ($S = 0.4$) on the flow motion with the boundary conditions sets is demonstrated in Fig. 4(a). The streamlines tend to appear with high intensity in the nanofluid layer and with two circulation cells on the interface. The flow circulation of the streamlines cells for the nanofluid

$(\Psi_{min})_{bf} = -1.76$, $(\Psi_{min})_{nf} = -1.55$

(a) $Ra = 10^4$

$(\Psi_{min})_{bf} = -8.81$, $(\Psi_{min})_{nf} = -8.85$

(b) $Ra = 10^5$

$(\Psi_{min})_{bf} = -18.4$, $(\Psi_{min})_{nf} = -19.9$

(c) $Ra = 10^6$

Fig. 3. Streamlines (left) and isotherms (right) evolution by Rayleigh number for water–Cu at $Da = 10^{-3}$, $S = 0.5$, $\omega = 0°$, $\phi = 0$ (solid lines) and $\phi = 0.05$ (dashed lines).
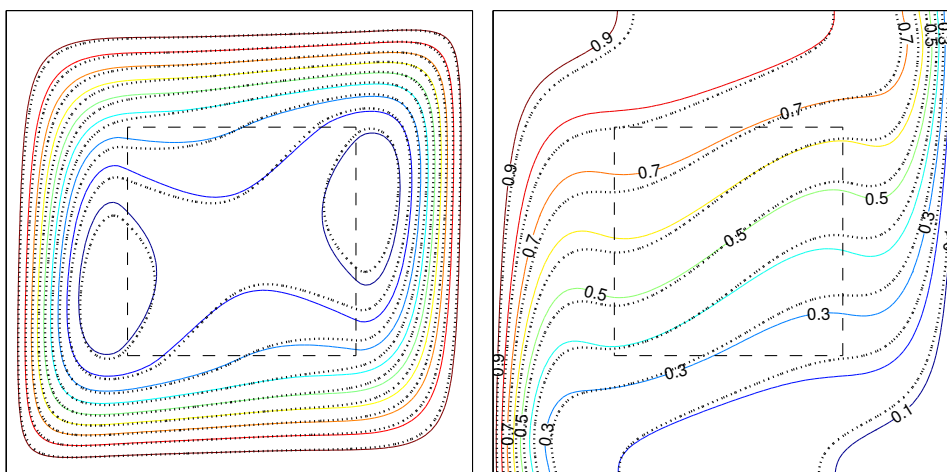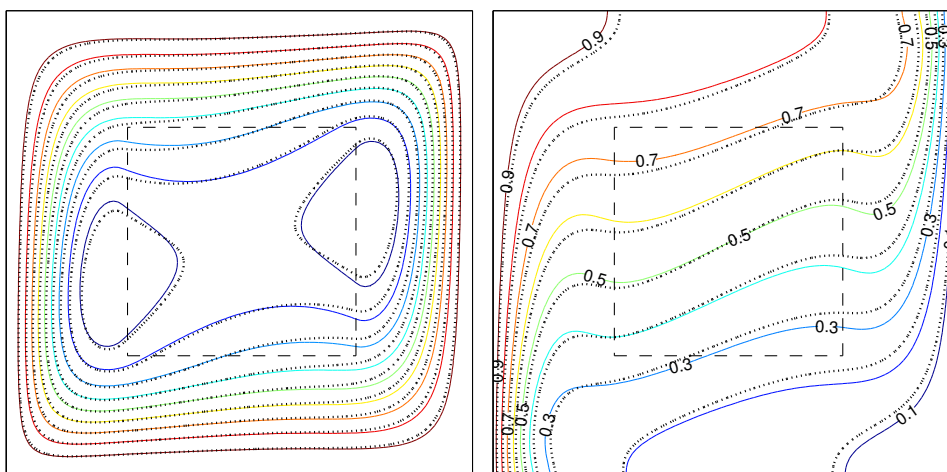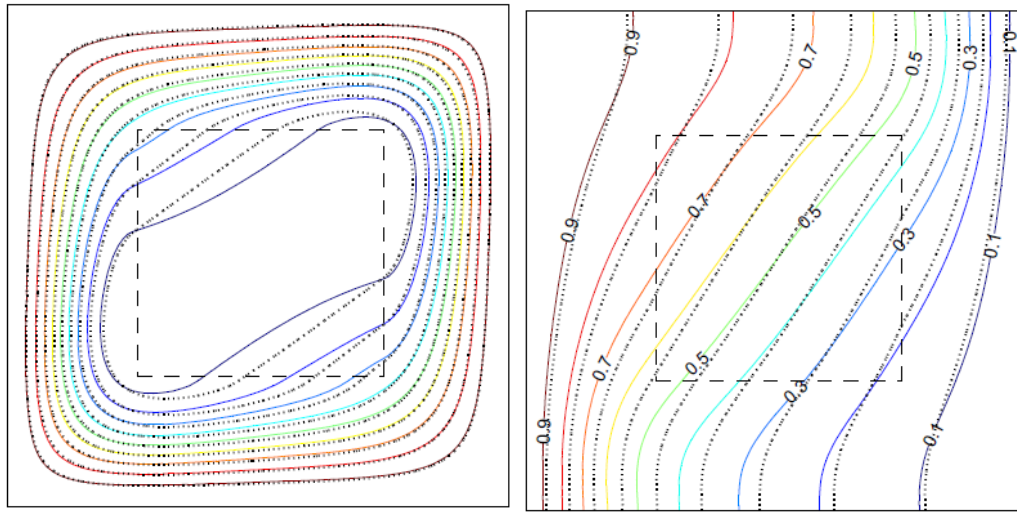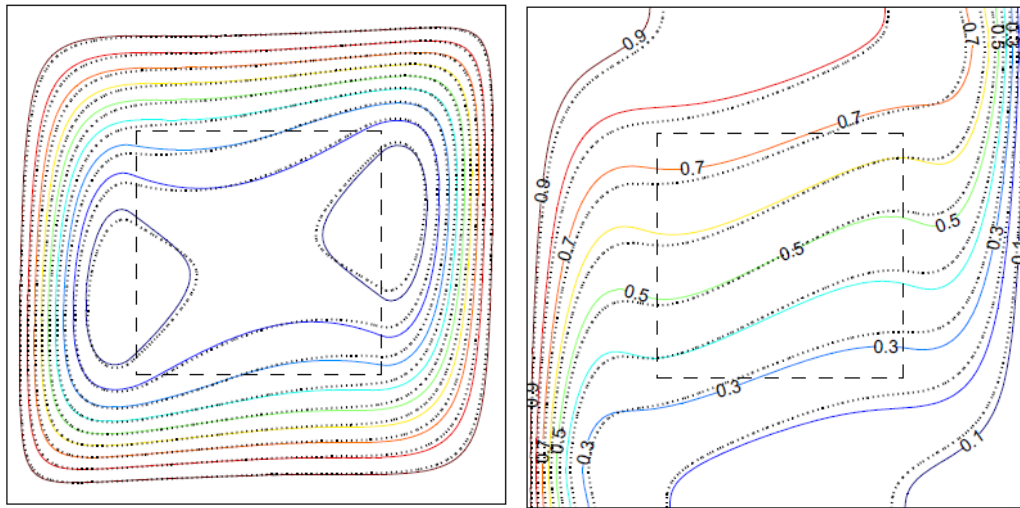
$(\Psi_{\min})_{bf} = -7.63$, $(\Psi_{\min})_{nf} = -7.56$

$(\Psi_{\min})_{bf} = -7.71$, $(\Psi_{\min})_{nf} = -7.65$

$(\Psi_{\min})_{bf} = -8.26$, $(\Psi_{\min})_{nf} = -8.3$
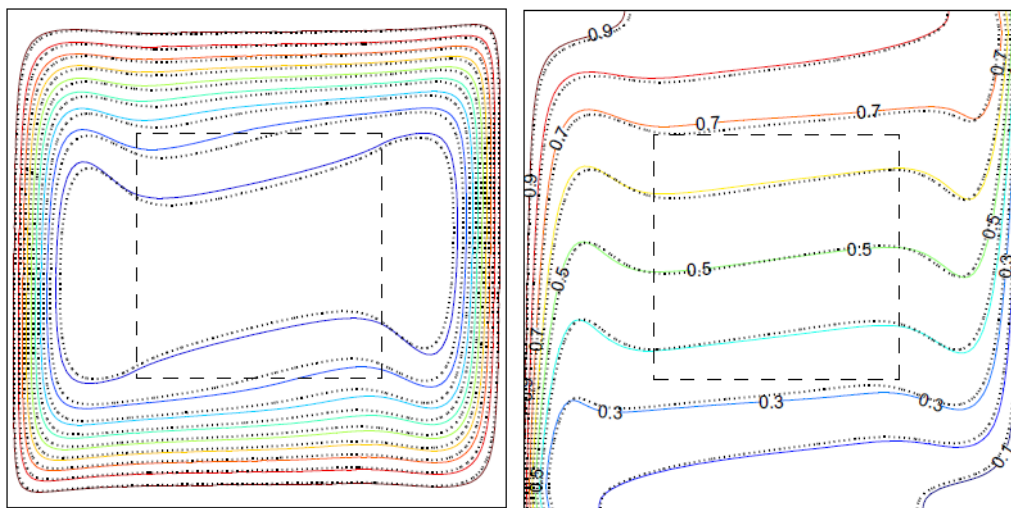
(a) $Da = 10^{-5}$

(b) $Da = 10^{-4}$

(c) $Da = 10^{-3}$

Fig. 4. Streamlines (left) and isotherms (right) evolution by Darcy number for water–Cu at $Ra = 10^5$, $S = 0.5$, $\omega = 0°$, $\phi = 0$ (solid lines) and $\phi = 0.05$ (dashed lines).
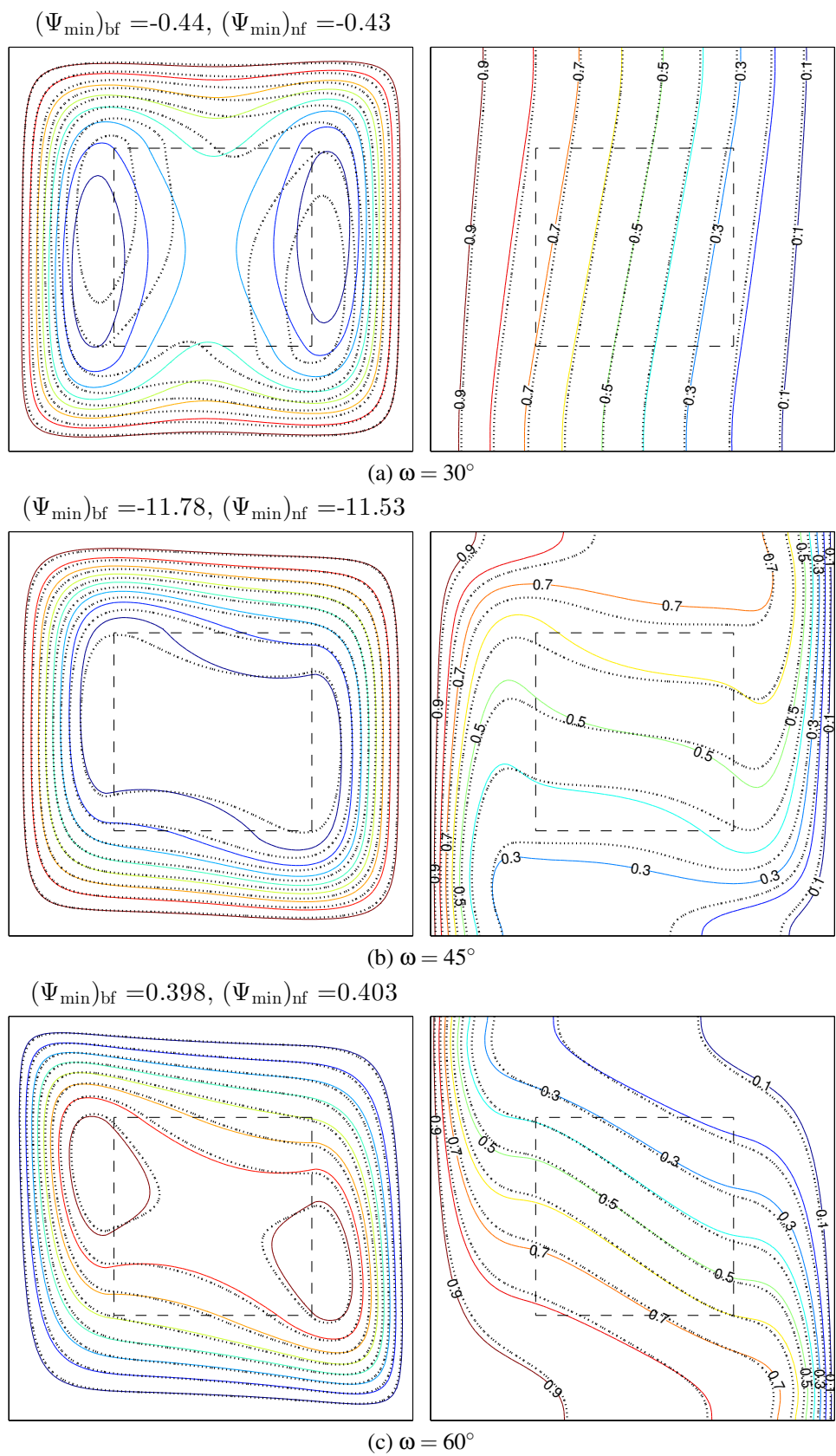
(b) $S = 0.4$

(c) $S = 0.6$

(d) $S = 0.8$

Fig. 5. Streamlines (left) and isotherms (right) evolution by fluid layer thickness for water–Cu at $Ra = 10^5$, $Da = 10^{-3}$, $\omega = 0°$, $\phi = 0$ (solid lines) and $\phi = 0.05$ (dashed lines).

1770

$(\Psi_{min})_{bf} = -0.44$, $(\Psi_{min})_{nf} = -0.43$

(a) $\omega = 30°$

$(\Psi_{min})_{bf} = -11.78$, $(\Psi_{min})_{nf} = -11.53$

(b) $\omega = 45°$

$(\Psi_{min})_{bf} = 0.398$, $(\Psi_{min})_{nf} = 0.403$

(c) $\omega = 60°$

Fig. 6. Streamlines (left) and isotherms (right) evolution by inclination angle of the cavity for water–Cu at $Ra = 10^5, Da = 10^{-3}, S = 0.5, \phi = 0$ (solid lines) and $\phi = 0.05$ (dashed lines).

is closer to that of pure fluid. The strength of the flow circulation increases (see Ψ_{min} values) after the addition of the nanofluid, due to the increase in thermal conductivity. The flow circulation of the streamlines cells for pure fluid are bigger than that for nanofluid. By increasing thickness of the fluid layer ($S = 0.6$), the streamline intensity into the fluid layer increases, affected by the resistance of the nanofluid (porous layer) hydrodynamic. The two circulation cells on the interface tend to disappear for the nanofluid, while for the pure fluid the cells shrink when they transform into the Multiplication shape. The strength of the flow circulation decreases for both pure fluid and nanofluid with the increasing value of S (see Ψ_{min} values), due to the resistance of the hydrodynamic nanofluid layer. The movement of the horizontal isotherm patterns into the fluid layer tend to take a diagonal shape, enhanced by the convection heat transfer, while the movement of the isotherm patterns into the nanofluid layer becomes more diagonal as S increases, as illustrated in Fig. 5(b). At a higher S value ($S = 0.8$), the streamlines are significantly affected; the two circulation cells into the fluid layer become one elliptical cell in the cavity centre for both nanofluid and pure fluid. The isotherm patterns tend to appear vertically and become more dense closer to the vertical (hot and cold) walls, while into the fluid layer tend to cause them to take the diagonal shape, as shown in Fig. 5(c).

The effect of the inclination angle of the cavity on the streamlines (left) and isotherms (right) is presented in Fig. 6. for water–Cu nanoparticles, $Ra = 10^5$, $Da = 10^{-3}$ and $S = 0.5$. The lower effect of ω ($\omega = 30°$) on the flow motion with the boundary conditions sets is demonstrated in Fig. 6(a). The streamlines tend to appear with high intensity into the fluid layer and with two circulation oval cells close to the interface. The flow circulation of the streamlines cells for pure fluid are bigger than that for nanofluid. The strength of the flow circulation for the streamlines in the clockwise direction decreases by applying 5% of Cu nanoparticles (see Ψ_{min} values). The isotherms patterns within the nanofluid layer and fluid layer tend to take a vertical shape due to the effect of the inclination angle. Increasing ω value to $45°$ tends to affect the streamlines, the two cells of the streamlines have a tendency to become one cell along the fluid layer. The strength of the flow circulation for the streamlines increases by increasing ω and the flow circulation of the streamlines cells for pure fluid tend to become closer to that of nanofluid. The isotherms pat-
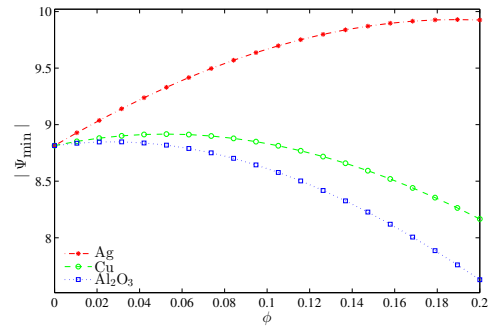

Fig. 7. Variation of the strength of the streamlines interfaces with the volume fraction for different nanoparticles at $Ra = 10^5$, $Da = 10^{-3}$, $S = 0.5$ and $\omega = 0°$.
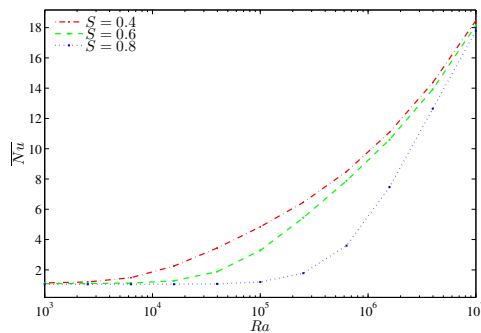
terns within the nanofluid and fluid layer are significantly affected by increasing ω. When moving into the fluid layer, the isotherms patterns take the shape of horizontal lines, while when they are near to the non-adiabatic (left and right) walls, the isotherms patterns appear vertically. The high increase of ω ($\omega = 60°$) affects the streamlines, the singular streamlines cell along the adiabatic (top and bottom) walls tend to becomes two cells on the interface walls. The strength of the flow circulation is switched into the anti-clockwise direction (positive signs of Ψ) by the increase of ω. The isotherms patterns within the cavity tend to take a diagonal shape and appear from the opposite direction of the vertical walls, as illustrated in Fig. 6(c).

Figure 7 shows the effect of various nanoparticles on the strength of the streamlines with nanoparticle volume fractions for $Ra = 10^5$, $Da = 10^{-3}$, $S = 0.5$ and $\omega = 0°$. We observe different behavior of the fluid flow by considering various nanoparticles affected by the viscosity forces and the inertial force. The strength of the flow circulation increases by adding Ag nanoparticle due to thermal conductivity increment which leads to strong inertial force. Adding Cu and Al_2O_3 nanoparticles tend to decrease the strength of the flow circulation due to the lower thermal conductivity. The significant enhancement appears on the strength of the streamlines obtained by higher nanoparticle volume fractions ($\phi \geq 0.1$).
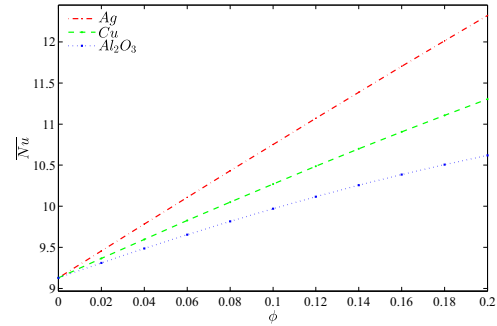
Figure 8 summarizes the variations in the average Nusselt numbers with Rayleigh number for different nanoparticle volume fractions of water–Cu at $Da = 10^{-3}$, $S = 0.5$ and $\omega = 0°$. Naturally, the convection heat transfer is increased with the rise of Rayleigh number. A higher concentration of nanoparticle volume fractions ($\phi = 0.2$) leads to a higher average
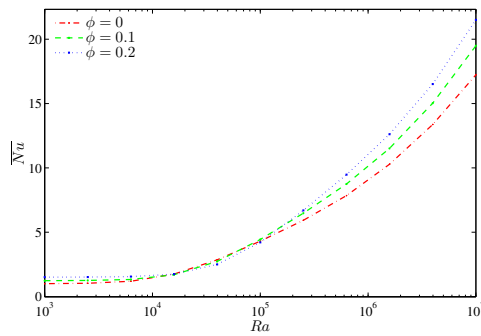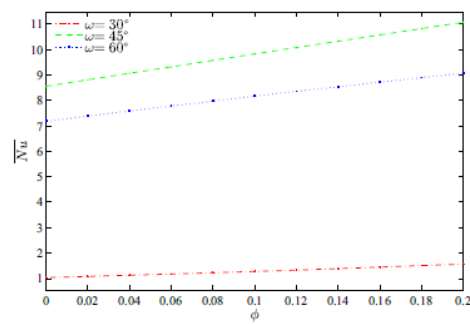
Fig. 8. Variation of the average Nusselt number interfaces with *Ra* for different ϕ at $Da = 10^{-3}$, $S = 0.5$ and $\omega = 0°$.

Fig. 10. Variation of the average Nusselt number interfaces with ϕ for different nanoparticles at $Ra = 10^6$, $Da = 10^{-3}$, $S = 0.5$, and $\omega = 0°$.

Fig. 9. Variation of the average Nusselt number interfaces with *Da* for different *S* at $Da = 10^{-3}$, $\phi = 0.05$ and $\omega = 0°$.

Fig. 11. Variation of the average Nusselt number interfaces with ϕ for different ω at $Ra = 10^6$, $Da = 10^{-3}$ and $S = 0.5$.

Nusselt number, but this value tends to drop lower than other values ($\phi = 0$ and 0.1) when the concentration of Rayleigh number is between $[10^4, 10^5]$ due to the structure of the cavity. The significant enhancement in average Nusselt number appears with the high values of Rayleigh number ($Ra > 10^5$).

Figure 9 shows the effect of the fluid layer thickness on the average Nusselt number with Rayleigh number for water–Cu at $Da = 10^{-3}$, $\phi = 0.05$ and $\omega = 0°$. As a result, the convection heat transfer enhancement occurs significantly at high Rayleigh number ($Ra > 10^5$), whereas lower Rayleigh number values have less effect on the convection. As the Rayleigh number increases, the average Nusselt number increases. The smaller nanofluid thickness layer ($S = 0.4$) has stronger effect on the heat transfer rate which has a higher average Nusselt number due to the lower thermal conductivity of pure fluid compared to that of nanofluid.

Figure 10 depicts the effect of various nanoparticles on the average Nusselt number with nanoparticle volume fractions at $Ra = 10^6$, $Da = 10^{-3}$, $S = 0.5$ and $\omega = 0°$. Due to its

higher thermal conductivity, *Ag* helps water in transporting more heat compared to what it does with *Cu* and Al_2O_3 nanoparticles, also shown in Table 2. The weak enhancement appears in the convection by applying Al_2O_3 nanoparticle as the nanoparticle volume fraction increases, due to lower thermal conductivity of Al_2O_3. However, it can be seen that *Cu* transports marginally more heat than Al_2O_3.

A very interesting result on the effect of various inclination angle of the cavity on the average Nusselt number for water–Cu at $Ra = 10^6$, $Da = 10^{-3}$ and $S = 0.5$ can be seen in Fig. 11. We find that the average Nusselt number increases with the increase of the nanoparticle volume fractions, ϕ, due to high thermal conductivity of the nanofluid which transfer more heat than pure fluid. Furthermore, when the value of the inclination angle of the cavity is $\omega = 45°$, it has a strong enhancement in the heat transfer rate which has the maximum value of the average Nusselt number. Smaller inclination angle $\omega = 30°$ transfers less heat which has the minimum value of the average Nusselt number.

Figure 12 demonstrates the effect of various
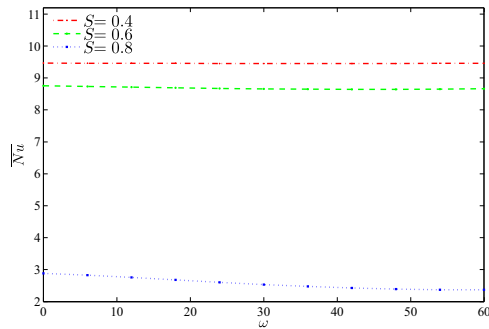
Fig. 12. Variation of the average Nusselt number interfaces with ω for different *S* at $Ra = 10^6$, $Da = 10^{-5}$ and φ = 0.05.

fluid layer thickness on the average Nusselt number with the inclination angle of the cavity for water–Cu at $Ra = 10^6$, $Da = 10^{-5}$, and φ = 0.05. As the inclination angle of the cavity increases, the heat transfer enhances due to the velocity changing. At lower *S* the average Nusselt number occurs with the maximum value, increasing ω tends to reduce the convection for the maximum *S* (*S* = 0.8) due to the lower thermal conductivity of pure fluid. For the minimum *S* (*S* = 0.4) and the increase of ω, the heat transfer rate is not affected.

5. CONCLUSION

Some important conclusions from the study are provided below:

1. It is found that when the nanoparticle volume fraction is applied, the circulation intensity increases due to the increase in the thermal conductivity of nanofluid. The conduction heat transfer pushes the isotherms patterns within the nanofluid layer to take an almost diagonal shape, while the convection mode heat transfer forces the isotherms patterns within the fluid layer to appear as horizontal lines on the vertical walls.

2. By increasing the nanofluid layer thickness, the transfer of streamline intensity into the fluid layer increases and this is affected by the resistance of the nanofluid (porous layer) hydrodynamic

3. A higher nanoparticle volume fraction (φ = 0.2) leads to a higher overall Nusselt number, but this value tends to drop lower than other values (φ = 0 and 0.1) when the concentration of Rayleigh number is between $[10^4, 10^5]$, due to the structure of the cavity.

4. The smaller nanofluid thickness layer (*S* = 0.4) has a stronger effect on the heat transfer rate which has a higher average Nusselt number due to lower thermal conductivity of pure fluid compared to that of nanofluid.

5. Qualitatively, the enhanced-heat transfer situation is seen in all the three nanoliquids compared to that of the base fluid but the following general result holds:

$$Nu^{water-Ag} > Nu^{water-Cu} > Nu^{water-Al_2O_3}.$$

6. The applications of this important result can be seen in the context of heat removal and heat storage systems like solar-energy systems and nuclear energy systems.

REFERENCES

Arani, A. A., M. Mahmoodi and S. M. Sebdani (2014). On the cooling process of nanofluid in a square enclosure with linear temperature distribution on left wall. *Journal of Applied Fluid Mechanics 7*(4), 591–601.

Beavers, G. S. and D. D. Joseph (1967). Boundary conditions at a naturally permeable wall. *Journal of Fluid Mechanics 30*(01), 197–207.

Beckermann, C., S. Ramadhyani and R. Viskanta (1987). Natural convection flow and heat transfer between a fluid layer and a porous layer inside a rectangular enclosure. *Journal of Heat Transfer 109*(2), 363–370.

Beckermann, C., R. Viskanta and S. Ramadhyani (1988). Natural convection in vertical enclosures containing simultaneously fluid and porous layers. *Journal of Fluid Mechanics 186*, 257–284.

Bhattacharya, P. and S. Das (2015). A study on steady natural convective heat transfer inside a square cavity for different values of rayleigh and nusselt numbers. *Journal of Applied Fluid Mechanics 8*(3).

Chamkha, A. J. and M. A. Ismael (2014). Natural convection in differentially heated partially porous layered cavities filled with a nanofluid. *Numerical Heat Transfer, Part A: Applications 65*(11), 1089–1113.

Chen, F. and C. Chen (1989). Experimental investigation of convective stability in a superposed fluid and porous layer when heated from below. *Journal of Fluid Mechanics 207*, 311–321.

Chol, S. (1995). Enhancing thermal conductivity of fluids with nanoparticles. *ASME-Publications-Fed 231*, 99–106.

Gobin, D., B. Goyeau and A. Neculae (2005). Convective heat and solute transfer in partially porous cavities. *International Journal of Heat and Mass Transfer 48*(10), 1898–1908.

Goyeau, B., D. Lhuillier, D. Gobin and M. Velarde (2003). Momentum transport at a fluid–porous interface. *International Journal of Heat and Mass Transfer 46*(21), 4071–4081.

Le Breton, P., J. Caltagirone and E. Arquis (1991). Natural convection in a square cavity with thin porous layers on its vertical walls. *Journal of Heat Transfer 113*(4), 892–898.

Nasrin, R. and M. Alim (2013). Free convective flow of nanofluid having two nanoparticles inside a complicated cavity. *International Journal of Heat and Mass Transfer 63*, 191–198.

Nessrine, Z., B. Ayda, D. Hcen and B. N. Sassi (2010). Flow and heat transfer during an expansion stroke in a composite fluid/porous system. *Journal of Applied Fluid Mechanics 3*(2), 87–95.

Poulikakos, D., A. Bejan, B. Selimos and K. Blake (1986). High rayleigh number convection in a fluid overlaying a porous bed. *International Journal of Heat and Fluid Flow 7*(2), 109–116.

Ramiar, A., A. Ranjbar and S. Hosseinizadeh (2012). Effect of axial conduction and variable properties on two-dimensional conjugate heat transfer of al2o3-eg/water mixture nanofluid in microchannel. *Journal of Applied Fluid Mechanics 5*(3), 79–87.

Singh, A. and G. Thorpe (1995). Natural convection in a confined fluid overlying a porous layer-a comparison study of different models. *Indian Journal of Pure and Applied Mathematics 26*, 81–95.

Vinogradov, I., L. Khezzar and D. Siginer (2011). Heat transfer of non-newtonian dilatant power law fluids in square and rectangular cavities. *Journal of Applied Fluid Mechanics 4*(2 -s 1), 37–42.

Webster, I., S. Norquay, F. Ross and R. Wooding (1996). Solute exchange by convection within estuarine sediments. *Estuarine, Coastal and Shelf Science 42*(2), 171–183.

Zaraki, A., M. Ghalambaz, A. J. Chamkha, M. Ghalambaz and D. De Rossi (2015). Theoretical analysis of natural convection boundary layer heat and mass transfer of nanofluids: Effects of size, shape and type of nanoparticles, type of base fluid and working temperature. *Advanced Powder Technology*.